

Particle current rectification in a quasi-periodic double-stranded ladder

Madhumita Saha¹ and Santanu K. Maiti^{1,*}

¹*Physics and Applied Mathematics Unit, Indian Statistical Institute,
203 Barrackpore Trunk Road, Kolkata-700 108, India*

(Dated: February 27, 2024)

We report transport properties and particle current rectification operation in a double-stranded tight-binding ladder network within non-equilibrium Green's function (NEGF) formalism that can easily be generalized in multi-stranded systems. First, we explore the rectification operation considering the model of an artificial double-stranded DNA (dsDNA) molecular system with Fibonacci type substitutional sequence. Substitutional sequences form quasi-periodic potentials. This analysis may shed new light in designing efficient nanoscale rectifier. It can also be directly implemented to different biomolecular systems like nucleic acids and most proteins as they follow quasi-periodic orders. Motivated with this fact, we consider different configurations depending on the choices of on-site energies and/or inter or intra strand nearest-neighbor hopping integrals in the form of Aubry-André-Harper (AAH) model (that also obeys quasi-periodic order), and in all the cases we find almost 100% current rectification even at very low bias region. Along with this, we observe that the phase (positive or negative) of rectification can suitably be engineered by tuning the Fermi energy and AAH phase. The effects of electron-electron (e-e) interaction and temperature are also studied, which show that a reasonably large rectification can be observed even for moderate temperature range and e-e interaction strength.

I. INTRODUCTION

Molecular systems will be the ultimate functional elements in fabricating electronic circuits at nanoscale level [1–3], suppressing the use of conventional conducting and semiconducting materials. The proposition of designing molecular diode or rectifier given by Ratner and co-workers essentially triggered the use of single molecules as active functional elements [4]. Later, some other theoretical proposals have been put forward describing the rectification action using simple and complex molecular systems [5–8]. However, a single molecular rectifier was first experimentally realized [9] in 2005 with modest rectification ratio (RR) ~ 10 . Since then the interest in this subject is rapidly growing up with considerable experimental and theoretical works [10–28]. Some of them are based on intrinsic properties [9–12] of the molecules, while the others have considered the effects of molecular coupling [13–16]. Instead of these significant advances, the present molecular diodes have had very limited applications especially due to their low conductances, low rectification ratio, high degree of sensitivity to junction configuration and much higher operating voltage [9, 10, 12, 13]. To circumvent these factors, few other works have been carried out [25–28] in order to get tunable rectification via gate voltage, environmental control, etc., though a successful conclusion is still lacking and thus further probing is undoubtedly required.

In the last few decades DNA molecules have attracted significant attentions in the fields of molecular physics and molecular spintronics due to their unique and diverse characteristic features [29–34]. Using DNA-coralyn complex molecule as a functional element Guo *et al.* [34] have shown that efficient rectification can be performed,

and the rectification ratio can be reached up to ~ 15 even at relatively small bias voltage (1.1 V). Artificial DNA sequences, those are usually constructed in a quasi-periodic manner, even also play appealing roles on transport phenomena, and several important aspects have already been revealed along this line considering different aperiodic lattices like Copper-mean, Nickel-mean, Fibonacci [35], Thou-Morse [36], and to name a few [33]. Appreciating the enormous possibilities of DNA molecule to become a role model in future nanoelectronic devices, can we now think about a DNA device where large asymmetry in current-voltage curves can be obtained and tuned externally? It has been established by us that a 1D chain with quasi-periodic potential can show strong rectification [37]. Naturally, it raises an obvious question that whether an artificial dsDNA which follows discrete quasi-periodic sequence can exhibit strong rectification. Fermi energy E_F is the only externally tunable parameter for this system which can be controlled by gate voltage. Now, in the search of other possible tuning parameters in an artificial DNA device, we consider a double-strand ladder network with quasi-periodic modulations [38–44] in the form of well-known Aubry-André-Harper (AAH) model [45]. Recently AAH model has got significant attention in both theoretical and experimental research [46–58]. The quasi-periodicity can be tuned with the help of AAH phase(s) [53] and the modulations can be incorporated in the diagonal and/or off-diagonal parts. Thus, in their unique characteristics, AAH models make them suitable candidates for designing efficient nanoscale devices, and in the present work, we explore how rectification operation can be performed considering a double-strand AAH ladder (Fig. 1) with E_F and the AAH phase.

The primary motivations of this work are as follows. First, we start with an artificial dsDNA molecular system with Fibonacci sequence to explore particle current rectification operation. If the rectification perfor-

*Electronic address: santanu.maiti@isical.ac.in

mance is good enough then we can argue that a double-stranded ladder with quasi-periodic sequence will be a functional element for designing nanoscale rectifiers since DNA molecule can be modeled nicely with quasi-periodic sequences, as already reported in many works [33, 38]. Following the DNA results, we attempt to propose a suitable model where much higher rectification can be obtained, and at the same time, the rectification ratio can be tuned externally by more parameters other than the gate voltage. In our model, there are two phase factors associated with the cosine modulations in diagonal as well as off-diagonal parts of the AAH Hamiltonian, which will play the key roles for effective controlling. We believe that rectification operation in quasi-periodic ladder network is quite interesting, and have not been discussed so far, to the best of our concern.

The essential mechanism of rectification relies on the fact that in presence of finite bias, a voltage drop takes place along the ladder. Therefore, average density of states (ADOS) and transmission spectrum become voltage dependent. The quasi-periodic potential leads to a gapped and fragmented spectrum [59, 60] and breaks the spatial reflection symmetry. It makes quasi-periodicity a key ingredient for occurrence of large particle current rectification [37]. In a recent work [61], strong energy current rectification has been shown in a quadratic bosonic system, subjected to quasi-periodic potential, which is connected to spin baths having differing temperatures. Within a tight-binding (TB) framework we investigate transport properties and particle current rectification operation using the Green's function formalism [62–67]. First, we investigate strong rectification in an artificial dsDNA molecule with Fibonacci sequence which forms quasi-periodic potential. The mechanism behind the rectification is solely due to the quasi-periodicity and it is completely different from the previous work on DNA molecule done by Guo and co-workers [34]. Then, different cases are taken into account depending on the specific choices of site energies and/or nearest-neighbor hopping (NNH) integrals in the form of AAH modulations. In all the cases high degree of rectification is obtained, which on one hand appears at sufficiently low bias, and, on the other hand, sustains for a wide range of parameter values. We find that the RR can be tuned significantly by modulating the AAH phase, keeping the E_F constant. This is one of the key advantages of AAH model over other discrete quasi-periodic systems. We also discuss the effects of electron-electron (e-e) interaction, treated at the Hartree-Fock (HF) mean-field (MF) level [68–71], and temperature. We find that the asymmetry in current-voltage curves persists over a moderate temperature range and for different values of interaction strength. We hope that the present analysis can be verified in future with suitable experimental setup.

The rest of the work is organized as follows. In Sec. II we present the model, TB Hamiltonian and theoretical framework for the calculations. The results are thoroughly analyzed in Sec. III, and, few contemporary parts are discussed in Appendix A and Appendix B. Finally, we conclude our findings in Sec. IV.

II. MODEL, TB HAMILTONIAN AND THE THEORETICAL FRAMEWORK

A. Model and the Hamiltonian

Let us begin with Fig. 1, where a double-strand ladder is coupled to source (S) and drain (D) electrodes. The channel-I and channel-II describe the two strands of

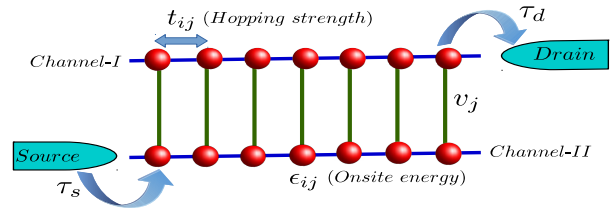


FIG. 1: (Color online). Junction setup where a double-strand ladder is coupled to source and drain electrodes.

the ladder those are directly connected through vertical bonds (the so-called rungs). We describe the junction using a TB framework and within this framework the TB Hamiltonian of the full system can be written as a sum $H = H_{ladder} + H_{elec} + H_{tunn}$, where H_{ladder} represents the Hamiltonian of the ladder, H_{elec} corresponds to the Hamiltonian of the side-attached electrodes, and H_{tunn} is associated with the tunnel coupling between the ladder and electrodes.

In absence of e-e interaction, the TB Hamiltonian of the ladder under NNH approximation reads as

$$H_{ladder} = \sum_{i=I,II} \sum_j \epsilon_{ij} c_{ij}^\dagger c_{ij} + \sum_{i=I,II} \sum_j t_{ij} c_{ij}^\dagger c_{i,j+1} + \sum_j v_j c_{I,j}^\dagger c_{II,j} + h.c. \quad (1)$$

Here, the index i refers to the strands and j represents the sites in each strand. The ladder is parameterized with on-site energy ϵ_{ij} , intra-strand NNH integral t_{ij} and the inter-strand NNH integral v_j . c_{ij}^\dagger (c_{ij}) is the Fermionic creation (annihilation) operator at site (i, j) . In presence of non-zero bias, a finite bias drop takes place along the ladder and the actual variation of this potential profile is very hard to execute since it involves a complete many-body problem. But, we can introduce this effect ‘phenomenologically’ into our Hamiltonian, as already proposed earlier in other works [34, 37, 72–74], considering different kinds of potential variation. The most common form of it is the linear dependence, and in our work we also consider this variation, though some other forms are also taken into account associated with electron screening in different materials. With these different choices only the quantitative behavior changes slightly, whereas the qualitative features remain unchanged. Now, in presence of a finite bias drop along the ladder its site energy becomes $\epsilon_{ij} = \epsilon_{ij}^0 + \epsilon_{ij}^V$, where ϵ_{ij}^0 represents the site energy in absence of bias voltage V , while ϵ_{ij}^V is the voltage dependent term. Assuming a linear bias drop, the voltage dependent site energy becomes $\epsilon_{ij}^V = V/2 - jV/(N+1)$,

where N represents the total number of rungs in the ladder.

To describe the electronic transport and rectification operation, we connect the ladder with two reflectionless 1D electrodes. The Hamiltonian of the electrodes, parameterized with on-site energy ϵ_0 and NNH integrals t_0 looks like

$$H_{elec} = \epsilon_0 \sum_i b_{iS(D)}^\dagger b_{iS(D)} + t_0 \sum_i b_{iS(D)}^\dagger b_{i+1S(D)} + h.c. \quad (2)$$

where $b_{iS(D)}^\dagger$ ($b_{iS(D)}$) is the creation (annihilation) operator in the electrodes.

The last part of the Hamiltonian of the full system i.e., the TB Hamiltonian associated with the tunnel coupling can be expressed as

$$H_{tunn} = \tau_s b_{-1S}^\dagger c_{I1} + \tau_d c_{II,2N}^\dagger b_{1D} + h.c. \quad (3)$$

where τ_s and τ_d are the coupling strengths of the source and drain electrodes with the ladder, respectively. In numbering the atomic sites of a N -rung ladder, we use site number 1 where the source is coupled, while the end site number is $2N$ where the drain is connected.

B. Interacting model

The interacting TB Hamiltonian for the ladder neglecting the spin degrees of freedom looks like

$$\begin{aligned} H_{ladder} = & \sum_{i=I,II} \sum_j \epsilon_{ij} c_{ij}^\dagger c_{ij} + \sum_{i=I,II} \sum_j t_{ij} c_{ij}^\dagger c_{i,j+1} \\ & + \sum_j v_j c_{I,j}^\dagger c_{II,j} + h.c + u \sum_{i=I,II} \sum_j n_{ij} n_{i,j+1} \\ & + u_1 \sum_j n_{Ij} n_{IIj} \end{aligned} \quad (4)$$

where u and u_1 are the nearest-neighbor intra-strand and inter-strand Coulomb repulsion energy strengths, respectively, and $n_{i,j}$ is the number operator. For this open quantum system, we treat the interaction term within the Hartree-Fock MF approximation, where the occupation number at any site is calculated using self-consistent procedure [68–71]. Within this scheme, the interacting system is effectively treated as non-interacting one, and the HF Hamiltonian becomes

$$\begin{aligned} H_{ladder}^{HF} = & \sum_{i=I,II} \sum_j \epsilon'_{ij} c_{ij}^\dagger c_{ij} + \sum_{i=I,II} \sum_j t'_{ij} c_{ij}^\dagger c_{i,j+1} \\ & + \sum_j v'_j c_{I,j}^\dagger c_{II,j} + h.c. \end{aligned} \quad (5)$$

Here the modified on-site energies are related to the Hartree term and it gets the form $\epsilon'_{Ij} = \epsilon_{Ij} + u(\langle n_{I,j+1} \rangle + \langle n_{I,j-1} \rangle) + u_1 n_{II,j}$. Whereas, the modified hopping terms are related to the Fock exchange terms and they are: $t'_{ij} = t_{ij} - u \langle c_{i,j+1}^\dagger c_{ij} \rangle$ and $v'_j = v_j - u_1 \langle c_{II,j}^\dagger c_{Ij} \rangle$. The MF quantities $\langle n_{ij} \rangle$, $\langle c_{i,j+1}^\dagger c_{ij} \rangle$ and $\langle c_{II,j}^\dagger c_{Ij} \rangle$ are determined self-consistently using the NEGF formalism [70].

C. Theoretical framework for the calculations

To characterize transport properties and rectification operations, the first quantity that we need to calculate is the two-terminal transmission probability $T(E)$ (E being the energy of injected particles) across the junction. We evaluate it using the NEGF formalism [62–66], where the effects of side-attached electrodes are incorporated through self-energy corrections. The effective Green's function of the non-interacting ladder is written as:

$$G_{ladder}^r = [(E + i\eta)I - H_{ladder} - \Sigma_S^r - \Sigma_D^r]^{-1} \quad (6)$$

where $\eta \rightarrow 0^+$, and Σ_S^r and Σ_D^r are the retarded self-energy matrices due to S and D, respectively. From these self-energies, we calculate the coupling matrices Γ_S and Γ_D from the expression $\Gamma_{S(D)} = -2\text{Im}[\Sigma_{S(D)}^r]$. Using Γ_S and Γ_D we compute two-terminal transmission probability following the Fisher-Lee relation[62], and, it is written in the form

$$T = \text{Tr}[\Gamma_S G_{ladder}^r \Gamma_D G_{ladder}^a] \quad (7)$$

where $G_{ladder}^a = (G_{ladder}^r)^\dagger$.

In presence of e-e interacting, the Green's function gets modified by $G_{ladder}^{HF,r}$ and it becomes,

$$\mathcal{G} = G_{ladder}^{HF,r} = [(E + i\eta)I - H_{ladder}^{HF} - \Sigma_S^r - \Sigma_D^r]^{-1} \quad (8)$$

\mathcal{G} is a $2N \times 2N$ matrix and it is written in (i, j) basis. Here i has two values I and II and j runs from 1 to N . We calculate the different MF quantities $\langle n_{ij} \rangle$, $\langle c_{i,j+1}^\dagger c_{ij} \rangle$ and $\langle c_{II,j}^\dagger c_{Ij} \rangle$ from the integration $(1/2\pi) \int M_{pq} dE$ where M_{pq} is the pq (associated with the indices i and j) element of the matrix $M = \mathcal{G}^\dagger (\Gamma_S f_S + \Gamma_D f_D) \mathcal{G}$. f_S and f_D are the Fermi distribution functions for S and D, respectively. Using self-consistent procedure, we get the converged G_{ladder}^{HF} . For this interacting system, we calculate the transmission probability $T(E)$, similar to the non-interacting one through the expression

$$T = \text{Tr}[\Gamma_S G_{ladder}^{HF,r} \Gamma_D G_{ladder}^{HF,a}] \quad (9)$$

In order to inspect the nature of energy bands under different biased conditions which is extremely crucial for analyzing rectification mechanism we need to compute ADOS, and we perform it using the relation [63, 64]

$$\rho(E) = -\frac{1}{2N\pi} \text{Im}[\text{Tr}(G_{ladder}^r)] \quad (10)$$

where $2N$ gives the total number of lattice sites in a N -rung ladder. For the interacting case, G_{ladder}^r will be replaced by $G_{ladder}^{HF,r}$.

Finally, we compute transport current across the junction through the expression [63, 64]

$$I_T = \int dE [f_S(E) - f_D(E)] T(E) \quad (11)$$

Calculating the currents for two different polarities of external bias we eventually compute the rectification ratio (RR), and it is defined as

$$RR = \frac{|I_T(+V)| - |I_T(-V)|}{|I_T(+V)| + |I_T(-V)|} \quad (12)$$

$RR = 0$ corresponds to no rectification, whereas $RR = 1$ or $RR = -1$ represents 100% rectification, depending on which current is fully suppressed in a particular bias polarity.

III. NUMERICAL RESULTS AND DISCUSSION

In what follows we present our results. We measure all the energies in unit of electron-volt (eV). Throughout the analysis we choose site energies of the electrodes $\epsilon_0 = 0$ and NNH integrals $t_0 = 3$, unless specified otherwise, and present I_T - V curves in log-linear plot, for better viewing.

A. DNA molecule

First, we want to look into the behavior of current rectification for an artificial dsDNA molecule. It is modeled by a two stranded tight-binding ladder (see Fig. 2) considering the four nitrogenous bases, Adenine (A), Guanine (G), Thymine (T) and Cytosine (C). We choose the site energies of these bases as $\epsilon_G = 8.3$, $\epsilon_A = 8.5$, $\epsilon_T = 9.0$, and $\epsilon_C = 8.9$. The horizontal hopping strengths between the same bases are $t_{GG} = 0.11$, $t_{AA} = 0.22$, $t_{CC} = -0.05$, and $t_{TT} = -0.14$, while the horizontal hopping strengths between the different bases can be calculated using $t_{AG} = (t_A + t_G)/2$. The vertical hopping strength is set at $v_j = -0.3$ [33].

Thousands of various sequences can be composed from these bases A, T, G and C. While natural DNA molecules can be extracted from the cells of all living organisms, artificial DNA molecules could be fabricated in any desired sequence. The natural dsDNA is extracted from the sequence of human chromosome 22 (chr22). Human chromosome based sequences are hc1, hc2, hc3 and the sequences consist of the mixture of all the four bases. The man-made dsDNA is taken in the form of a random sequence as well as in substitutional form like nickel mean, copper mean, triadic cantor, Fibonacci, etc [33]. All these substitutional sequences are constructed following an inflation rule. For instance, starting from the base A, Fibonacci sequence can be formed by the rule $A \rightarrow AG$ and $G \rightarrow A$. Thus, the substitutional sequences for a strand are the mixture of two base pairs. Knowing the sequence for one single-strand, one can construct the sequence for the other strand satisfying the Watson-Crick (WC) base-pairing rules: G pairs with C, and A pairs with T [33]. The substitutional sequences form quasi-periodic potential. In Ref. [37], we have seen quasi-periodicity plays an important role behind large rectification in a 1D chain. Therefore, to construct the artificial dsDNA molecule, we arrange the bases A and G in the upper strand (i.e., channel-I) following a Fibonacci sequence (quasi-periodic

one), and the other strand is automatically designed with

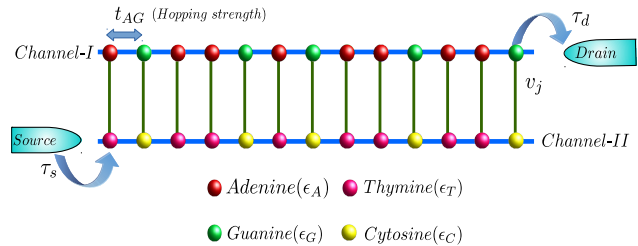


FIG. 2: (Color online). dsDNA model represented as two strand ladder with actual four bases like Adenine, Guanine, Thymine and Cytosine, is coupled to source and drain.

the bases T and C (which is also a quasi-periodic sequence) following the WC base-pairing rules [33]. To explore the rectification operation we connect the dsDNA molecule with the two electrodes (see Fig. 2), those are parametrized with on-site energy $\epsilon_0 = 0$ and NNH integrals $t_0 = 5$. The molecule-to-electrode coupling is fixed

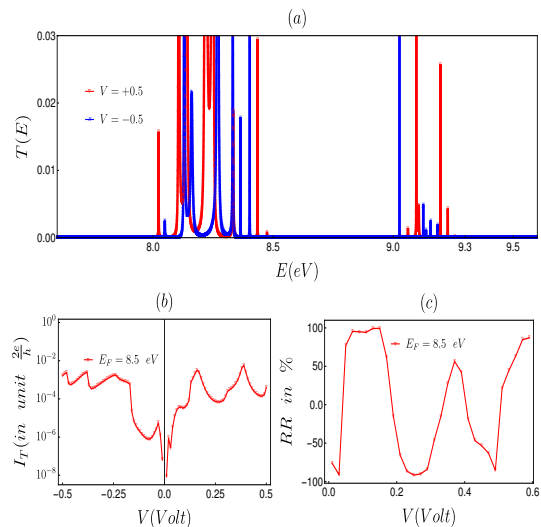


FIG. 3: (Color online). Results of the Fibonacci dsDNA molecule having 13 rungs where (a), (b) and (c) correspond to the transmission probability, junction current and the variation of rectification ratio.

at $\tau_s = \tau_d = 0.7$. The results for this molecular junction, computed at zero temperature and in the absence of e-e interaction, are placed in Fig. 3. Here we find distinct nature of transmission spectra under two bias polarities (Fig. 3(a)). In reversing the bias, the energy spectrum of the bridging system gets changed, as site energies are voltage dependent, which results different transmission spectra under two biased conditions. As the spectrum is gapped due to the quasi-periodic nature of site energies, one can definitely find a suitable Fermi energy E_F about which transmission is finite over a small energy window for one bias polarity, while it becomes vanishingly small or even zero for the other biased condition. This leads to a high degree of current rectification which is exactly shown in Figs. 3(b) and (c). At some specific

voltage regions almost 100% rectification ($RR \sim \pm 100\%$) is obtained, which has not been reported so far in literature. In their work Guo *et al.* [34] have shown that the artificially designed dsDNA with 11 base pairs, where three different bases are mixed (CGCGAAACGCG), cannot produce strong current rectification. But, after intercalating two coralyne molecules into the dsDNA one, the whole DNA-coralyne complex exhibits much stronger rectification. In comparison to dsDNA molecule, DNA-coralyne complex shows higher ‘spatial asymmetry’ at the left and right edges where electrodes are connected to the system. The striking spatial asymmetry induced by coralyne intercalation is the explanation for the strong rectification in the DNA-coralyne complex. In our model, the sequence of dsDNA molecule and the mechanism behind rectification are completely different from what is discussed in Ref. [34]. We show that the artificial dsDNA with Fibonacci type substitutional sequence exhibiting strong rectification depending on the gapped and fragmented nature of energy spectrum, solely depends the quasi-periodic behavior of substitutional sequence. For the other substitutional sequences also, it is possible to have the perfect current rectification as the physics behind rectification remains unchanged. It gives a clear signature that the artificial dsDNA molecule with substitutional sequences can be a suitable functional element for utilizing rectifying operation at nanoscale level. Other than the dsDNA, different bio-molecular systems like nucleic acids and most proteins follow the quasi-periodic orders [38]. As the quasi-periodicity gives rise to strong rectification, the other bio-molecular systems may also be implemented for strong rectification.

B. Ladder with AAH potential

As quasi-periodicity plays an important role in getting high degree of rectification, which is established from the results of DNA molecule, now we focus our attention on the current rectification considering an AAH ladder. It may provide an additional advantage as the rectification ratio can be tuned *externally* with the AAH phase, which is always helpful in designing a device. AAH potential is also a quasi-periodic potential and it has the form $\epsilon_i = W \cos [2\pi bi + \phi_\beta]$ [45]. Here W is the strength of the potential, ϕ_β is the phase associated with the AAH modulation, and, b is an irrational number. It is important to note that the phase factor ϕ_β does not change the behavior of transport, but it changes the location of the bands in presence of a linear potential drop. In our calculations we set $b = (1 + \sqrt{5})/2$, the golden mean, which is most commonly used, though any other irrational number can be taken into account and the physics will not be changed at all. Depending on the strength W , the AAH system contains extended, critical and localized states. Transport through the extended states are faster than the critical states. With increasing system size transport through critical states gets decreased, whereas for the extended ones as the transport is ballistic it does not depend on the size of the system. This is one of key the

advantages of the AAH type quasi-periodic sequence over the other quasi-periodic sequences like Fibonacci, Thue-Morse, etc., as these discrete quasi-periodic sequences only possess critical single particle eigenstates [59].

An AAH ladder can in principle be designed by incorporating AAH modulations in different parts like on-site energies and/or inter or intra strand NNH integrals. Now we will focus on a specific configuration where we set $\epsilon_{Ij}^0 = W \cos [2\pi bj + \phi_\beta]$, $\epsilon_{IIj}^0 = 0$, $t_{Ij} = t_{IIj} = t$ and $v_j = v, \forall j$.

1. Rectification

To show the rectification behavior, in Fig. 4(a) we show the variation of transmission probabilities of a ladder network at a typical bias voltage under forward and reverse bias conditions. At a first glance we see that the transmission spectra are quite different for two distinct polarities of the external bias, providing sharp resonant peaks at multiple energies. A careful inspection reveals that there are some (small) energy windows where finite transmission is obtained only due to one bias polarity, while the transmission gets almost suppressed in other

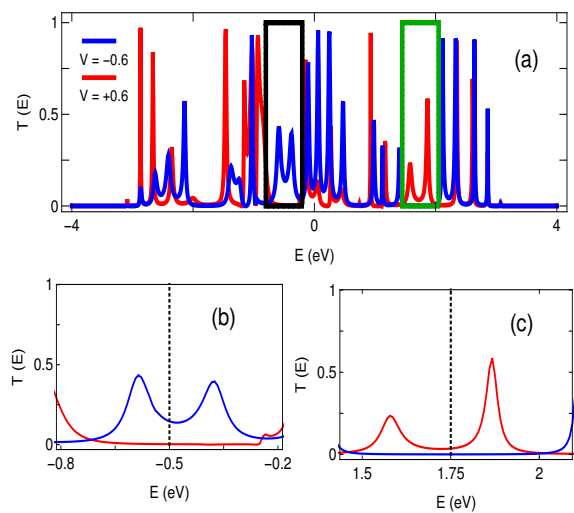


FIG. 4: (Color online). (a) Two-terminal transmission probability as a function of energy for a 13-rung ladder under forward and reverse bias conditions, where the red and blue lines correspond to $V = 0.6$ V and -0.6 V, respectively. The spectra given in (b) and (c) represent the enlarged versions of the black and green framed regions of (a), respectively, for clear viewing of different colored curves in these two energy zones of our interest. The imaginary dotted lines in (b) and (c) are associated with the locations of Fermi energy. The other physical parameters taken for these calculations are: $t = 1$, $v = 1$, $W = 1$, $\phi_\beta = 0$, $\tau_s = 1$, and $\tau_d = 0.6$. Here we choose asymmetric conductor-to-electrode coupling.

bias condition, and this phenomenon will lead to much higher rectification. To examine this fact, we selectively choose two small energy zones from Fig. 4(a), marked by the black and green framed regions, and replot the enlarged versions in Figs. 4(b) and (c), respectively. In-

terestingly we see from these spectra (Figs. 4(b) and (c)) that, for the entire energy zones one curve (blue or red) dominates, whereas the other one almost vanishes. To

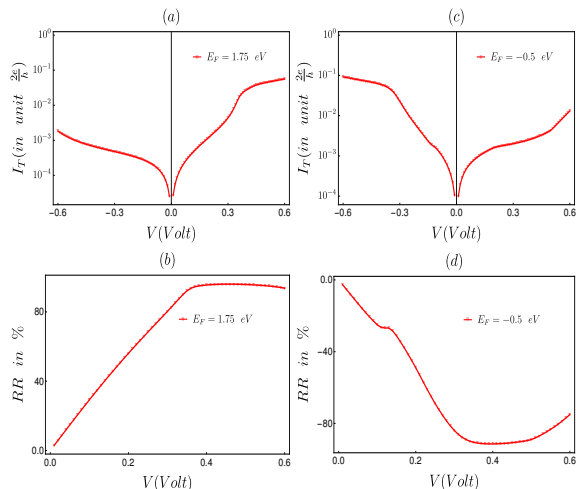


FIG. 5: (Color online). I_T - V and corresponding RR - V characteristics at two different Fermi energies for the AAH ladder considering the identical physical parameters as taken in Fig. 4.

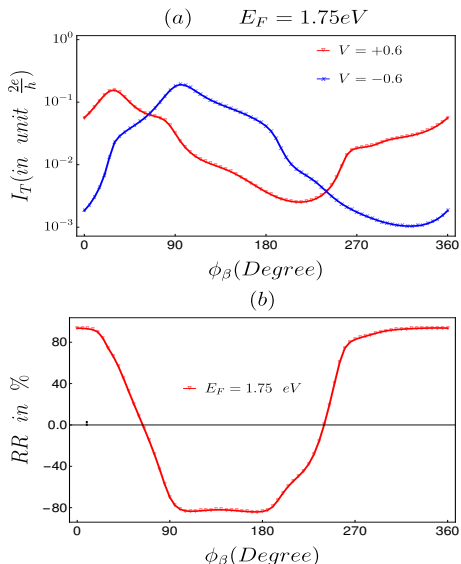


FIG. 6: (Color online). Role of AAH phase ϕ_β on transport current and rectification ratio. In (a), transport currents are shown for two bias polarities, represented by two different colored curves in a log-linear plot, and the corresponding RR is given in (b). Here we choose $E_F = 1.75$ eV, and all the other physical parameters are kept unchanged as taken in Fig. 4.

inspect the dependence of rectification for other voltages, let us focus on the spectra given in Fig. 5 where we calculate transport current along with rectification ratio by varying the voltage from zero to 0.6 V under two bias polarities, setting the Fermi energy at two suitable energies. For $E_F = 1.75$ eV, the transport current in the negative bias condition is vanishingly small, whereas much

higher current is obtained in the positive bias condition (see Fig. 5(a)). As a result of this, *very high degree of RR is achieved, and most remarkably, this feature persists over a broad range of voltage bias* (Fig. 5(b)). The phenomenon gets almost reversed when we set the Fermi energy at -0.5 eV, as clearly noticed from the spectra Figs. 5(c) and 5(d). Thus, E_F is one of the tuning parameters for regulating RR . If μ_1 and μ_2 are the chemical potentials of the source and drain, respectively, and V is the voltage bias maintained by the difference in chemical potentials, then we can write $\mu_1 = E_F + V/2$ and $\mu_2 = E_F - V/2$. In experiments, E_F is changed routinely in-situ by controlling external gate voltage [26].

In Fig. 6 we describe the critical role of the AAH phase ϕ_β on transport current and rectification ratio. The transport current is highly sensitive to the AAH phase, and currents are markedly different for two distinct bias polarities (see Fig. 6(a)). This behavior is clearly reflected in the RR - ϕ_β spectrum (Fig. 6(b)). From Fig. 6 we can see that *the RR achieves a very high value, close to 100%, and almost complete phase reversal (RR reaches to -100%) takes place upon the variation of ϕ_β . The other important feature is that the high degree of rectification persists over a wide range of the phase factor ϕ_β , that gives a clear hint that one can design a setup where ϕ_β can be selected from a reasonable window, and sharp tuning is no longer precisely required.* Here we would like to note that ϕ_β can be changed by designing different realizations of the on-site potential in a same experimental setup (details are obtained in the supplementary material of Ref. [48] and other works [49–51]).

2. Reason for 100% rectification

The large degree of rectification is caused due to the two reasons: (i) gapped fragmented spectrum and spatial reflection symmetry breaking of quasi-periodic potential, and (ii) voltage dependence of the energy levels due to the term ϵ_{ij}^V . Depending on these two factors, at zero temperature it is always possible to get a Fermi energy about which there is always an energy window where finite transmission is present for one biased condition and gapped for the other biased condition. This leads to 100% rectification which is clearly reflected from Fig. 4 and Fig. 5. The other possible reason of getting enhanced rectification can be in some cases due to the Wannier-Stark (WS) localization [75–77]. In presence of a non-zero bias, site energies are (electric) field dependent yielding a non-uniform distribution of the site energies which causes particle localization, analogous to a conventional disordered lattice, which is known as WS localization. The WS localization at finite bias can be seen from the spectra given in Fig. 4, and more clearly they can be visualized from the results presented in Fig. 7 as here we superimpose ADOS along with the transmission function. The red-dotted line is markedly different from the blue-dotted one associated with the energy shifting at two bias polarities. Where the dotted line (red and/or blue) vanishes (viz, states are no longer available), the transmission proba-

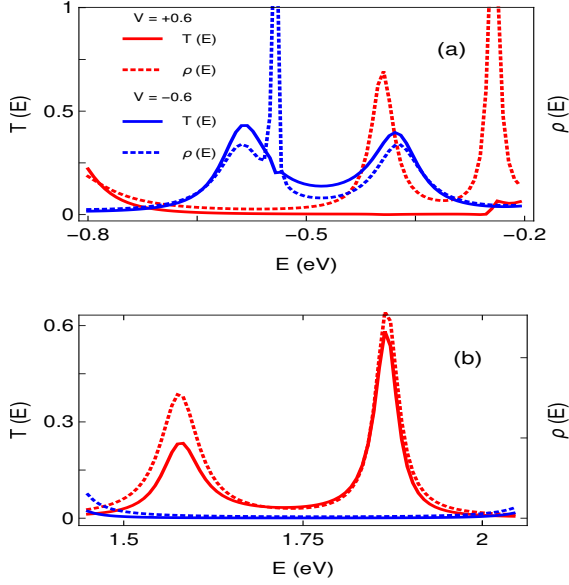


FIG. 7: (Color online). Transmission probability $T(E)$ and ADOS $\rho(E)$ for the two energy zones (shown in the upper and lower panels) as considered in Figs. 4(b) and (c), respectively. All the physical parameters are same as taken in Fig. 4.

bility naturally drops to zero. Whereas, for the energies when the transmission function vanishes irrespective of finite density of states we can conclude that the states associated with those energies are localized, and the localization is caused as a results of electric field (WS localization). Thus, finding of an energy zone (or more zones) where transmission probability is finite for one bias polarity and zero (or vanishingly small) for other polarity is always expected depending on the above reasons.

To the best of our knowledge, no one has addressed before this high degree of rectification, for such a wide range of bias voltage. Thus it brings a significant impact in the era of nanotechnology. At finite temperatures, the contributions from other energy zones will also appear which may reduce the rectification ratio, and we will discuss these issues in the forthcoming subsections.

To make the analysis more realistic and keeping in mind possible experimental realizations of the proposed model, we need to incorporate other different physical factors that may available in practical situations. Below we discuss these effects one by one as follows.

3. Critical roles of different physical factors on rectification

Here we want to address the effects system size, temperature and electron-electron interaction on current rectification, and to test how the above presented results are modified with these factors.

Effect of system size: As the energy spectrum of the AAH system is always gapped irrespective of the system size, we can still expect a very high degree of current rectification even for much bigger AAH ladder. To sub-

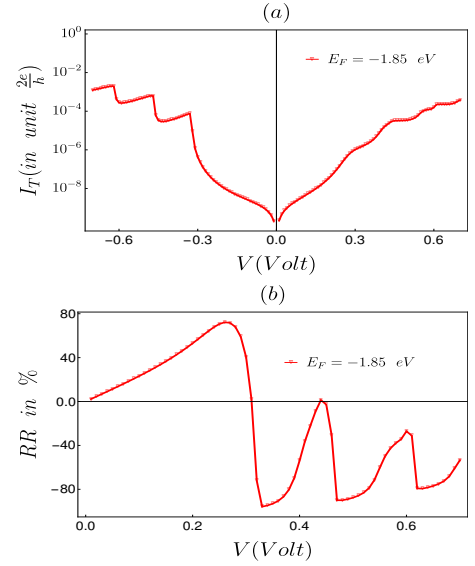


FIG. 8: (Color online). I_T and corresponding RR as a function of voltage bias for a bigger AAH ladder with 55 rungs (110 sites). Here we choose $E_F = -1.85$ eV. The other parameters are same as taken in Fig. 4.

stantiate this fact in Fig. 8 we plot the transport current and corresponding rectification ratio considering a bigger ladder with 55 rungs (110 sites). A high degree of rectification is clearly noticed for this ladder, and thus we can suggest that the basic features of rectification are not restricted within a specific system size, rather we can vary it in wide range which gives a suitable hint for testing the results in a laboratory setup.

Effect of temperature: The results studied so far are worked out at absolute zero temperature. Now, we include the effect of temperature and study the characteristic features of rectification. The results are shown in Fig. 9 where we plot the RR as a function of system tem-

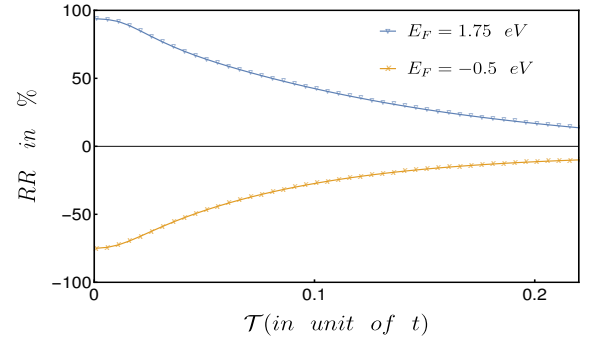


FIG. 9: (Color online). Temperature dependence of rectification ratio. The Fermi energies and other parameters are chosen as in Fig. 4.

perature for two different Fermi energies. The RR gets decreased with the enhancement of temperature. Though it (RR) gets reduced, still sufficiently large RR persists over a moderate range of temperature. This reduction of the degree of rectification can be implemented from the

argument that at finite temperature we need to incorporate all the energy levels in the allowed energy window, unlike the case of zero temperature which excludes the possibility of integrating transmission function in a specific energy window where finite transmission is obtained for one bias polarity. Thus, it is no longer possible to get absolutely 100% rectification since finite contributions from both the bias polarities are involved.

Effect of electron-electron interaction: Finally, we include electron-electron (e-e) interaction into the system and study its effect on rectification. We incorporate this effect at the MF level. It is well-known that the study of an open interacting system is a state-of-the-art research problem at formalism level. Even in the MF limit, one needs to do numerical integrations of the NEGF to evaluate the MF quantities, which is an extremely challenging task especially for large size systems exhibiting fragmented energy spectrum. Due to this fact here we restrict ourselves to the small system size. We present the results in Fig. 10 for an AAH ladder considering five rungs at some typical values of interaction strengths. The key feature is that, at some typical values of e-e interaction, there is a finite possibility to achieve a very high degree of rectification compared to the interaction free system, which is clearly visible from Fig. 10(b). It immediately raises an obvious curiosity that how the degree of rectification modifies with the gradual change of e-e interaction strength. To scrutinize it in more detail, in Fig. 10(c) we plot the rectification ratio by continuously varying the strength of u ($= u_1$) in a wide range. From the spectrum, it is clear that even in presence of electron-electron interaction (u, u_1), it is possible to have finite current rectification. Thus, at the MF level we can see that e-e interaction does not suppress the rectification action, rather better performance could be expected for some typical values of u (u_1). To estimate these specific values, more detailed analysis should be required and we leave this job for our future works.

Here we would like to note that, as already stated above, the computations of mean-field quantities are heavy for large interacting systems, and thus, we present the results considering a small size ladder. But, the essential physics will remain same for a reasonably large system as well, since the degree of rectification is essentially depends of the ratio of currents under two bias polarities. When the system size is very small, comparable to a quantum dot (QD), one may expect the effect of Coulomb blockade [78–80], especially for the situation when longer-range interactions are present and the system temperature is very low. In presence of this effect, although the electrical conductance, and thus, the junction current gets reduced, we do not expect any non-trivial feature in the degree of rectification as it involves the ratio of two currents which are equally affected by Coulomb repulsion. The same argument is also valid even if we consider the precise role of Coulomb drag [81–83] in our analysis. This dragging mechanism is generally expected when the two layers or channels are sufficiently close to each other, typically within the range of 1-2 nanometers. So, in one situation we may think that if we design an

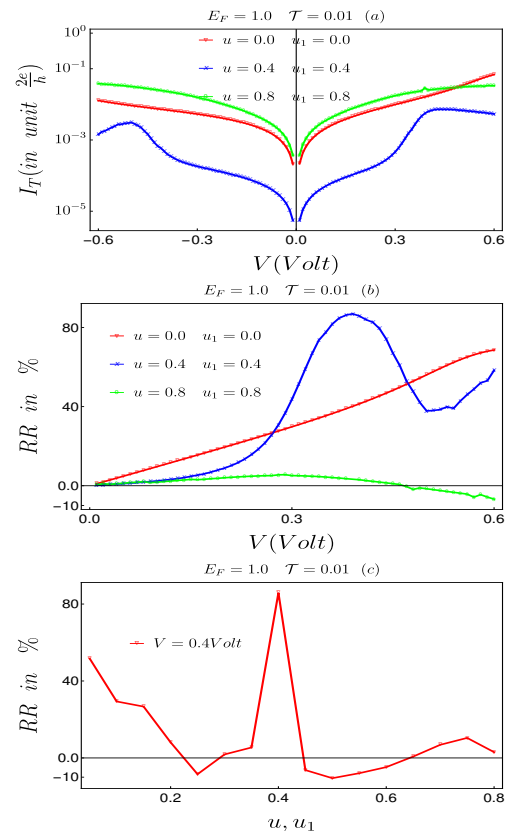


FIG. 10: (Color online). Transport current I_T in (a) and the corresponding RR in (b) as a function of bias voltage for some typical strengths of u and u_1 . In (c), the variation of RR with u ($= u_1$) is shown when the bias voltage is fixed at $V = 0.4$ V. The results are computed for a AAH ladder with five rungs setting the temperature at 0.01 (in unit of v).

AAH ladder where two strands are well separated, we can safely ignore the effect of Coulomb drag. On the other hand, for the situation when both the two strands are close enough, Coulomb drag effect will be an important one which will modify the currents. But as the ratio of currents under two biased conditions are taken into account we expect similar kind of rectification operation.

In the sub-section III B, we consider a double-stranded ladder with AAH modulation in Channel-I. For this ladder we establish a complete rectification operation depending on the choice of Fermi energy E_F at zero temperature, solely due to the quasi-periodic nature of the potential. Thus, it is expected that employing quasi-periodicity in any segment of the ladder leads to complete current rectification at zero temperature. To check that we include quasi-periodicity in different segments of ladder and the results are critically analyzed in Appendix A and Appendix B. Similar kind of complete current rectification is noticed, depending on the choices of E_F . We also show that changing the arbitrary phase term in the continuous quasi-periodic potential, the magnitude and direction of the rectification ratio can be varied significantly. In sub-section a of Appendix A, we consider the AAH modulation only in the inter-strand hopping strengths. The phase of the AAH potential is referred as

ϕ_λ when we consider the modulation in hopping integrals. We take into account the AAH modulations in on-site energies (sub-section *b* of Appendix A), and, in intra-strand hopping integrals (sub-section *c* of Appendix A) of both the channels. In the previous cases, we consider AAH modulation either in the on-site potentials or in the hoppings. Quasi-periodicity can also be included both in the on-site potential and hopping strengths, and the combined effect of both the two phases, ϕ_β and ϕ_λ , leads to interesting behavior in particle current rectification. We explore it in detail in Appendix B.

IV. SUMMARY AND OUTLOOK

In this work, we have studied particle current rectification for a tight-binding double-stranded ladder using NEGF formalism with discrete and continuous quasi-periodic potentials. We have started our analysis with an artificial dsDNA molecule which has Fibonacci type of substitutional sequence. This is a discrete quasi-periodic potential. The quasi-periodicity yields gapped and fragmented spectrum, which, in turn, leads to complete rectification on tuning the gate voltage at zero temperature for this artificial dsDNA. This is a new mechanism of getting rectification, and it greatly differs from the previous works (such as [34]) available in literature. Other biomolecular systems like nucleic acids, most of the proteins are also made up of quasi-periodic sequences. Our work thus suggests that they can also be used as functional elements to get suitable rectifications.

In the next part we have considered a double-stranded ladder with the continuous quasi-periodic AAH potential instead of discrete Fibonacci sequence. This system has two added advantages. Discrete quasi-periodic systems exhibit ‘critical’ (intermediate between extended and localized) wave functions. Transport through such wave-functions decreases with increase in system size. A system with a weak AAH potential provides completely extended wave functions, while also having gapped and fragmented spectrum those are required for current rectification. The transport through such extended wave functions is ballistic and does not depend on the system size. The AAH potential has a phase factor, which does not change the transport behavior, but changes the location of the bands in presence of a linear potential drop. Thus, this phase factor in the potential can serve as an additional tuning parameter for the regulation of current rectification, unlike the discrete quasi-periodic sequences where Fermi energy acts as the only controlling parameter. The AAH phase can be changed by design. As, the rectification behavior is governed by the quasi-periodicity, we have found complete rectification introducing quasi-periodicity at different segments of the ladder network. Non-interacting systems with AAH quasi-periodic potential have been realized experimentally [48–51]. Our results point to the possibility of large tunable rectification in such experiments.

Apart from complete rectification, another very important salient feature we have explored is that the di-

rection of rectification can be changed just by controlling the gate voltage in such systems with discrete or continuous quasi-periodic potentials. Complete rectification due to quasi-periodicity occurs at zero temperature. But, in real experimental setups the effect of temperature is unavoidable. Considering finite temperature, we have shown that the rectification ratio gets decreased, but still it is possible to get a reasonable amount of rectification for a moderate range of temperature. Finally, we have considered the effect of nearest-neighbor repulsive interaction for spinless fermions at the mean-field level. The mean-field results suggest that the interaction leads to a reduction in transport, but still a finite rectification is possible depending on the interaction strength.

V. ACKNOWLEDGMENTS

MS would like to thank Archak Purkayastha for useful discussions and would like to acknowledge University Grants Commission (UGC) of India for her research fellowship. SKM respectfully acknowledges the financial support of the Science and Engineering Research Board, Department of Science and Technology, Government of India (Project File Number: EMR/2017/000504).

Appendix A: Different other configurations of AAH ladder

a. AAH modulation in inter-strand hopping

In this configuration, both the two strands are perfect (viz, $\epsilon_{Ij}^0 = 0$ and $\epsilon_{IIj}^0 = 0$) and the intra-strand hopping integrals are uniform i.e., $t_{Ij} = t_{IIj} = t \forall j$. For this network we introduce modulation in the inter-strand hopping integrals in the form: $v_j = W_1 \cos[2\pi bj + \phi_\lambda]$, where W_1 is the modulation strength and ϕ_λ is the phase factor that can be tuned selectively [53]. Similar to the case described in the main text, let us begin with the results given in Fig. 11(a) where two-terminal transmission probability is shown for two different bias polarities considering a 15-rung ladder network. Sharp resonant peaks are observed at some particular energies, and these peaks are grouped in such a way that three allowed transmitting zones are formed and they are separated by finite gaps. This is the general feature of AAH type lattices, and solely associated with the ADOS spectrum. The other interesting feature is that the transmission function is mirror symmetric upon the reversal of bias polarities, that will provide another advantage in rectification operation as discussed below.

From the spectrum Fig. 11(a), we find two selective energy zones (marked by the black and green framed regions) of equal widths across $E = 0$, where only one colored curve dominates suppressing the other one. These two framed regions are redrawn in the enlarged form in Figs. 11(b) and (c), where ADOS are superimposed along with the transmission functions under two bias polarities in each of the two spectra. Clearly we can see that for a

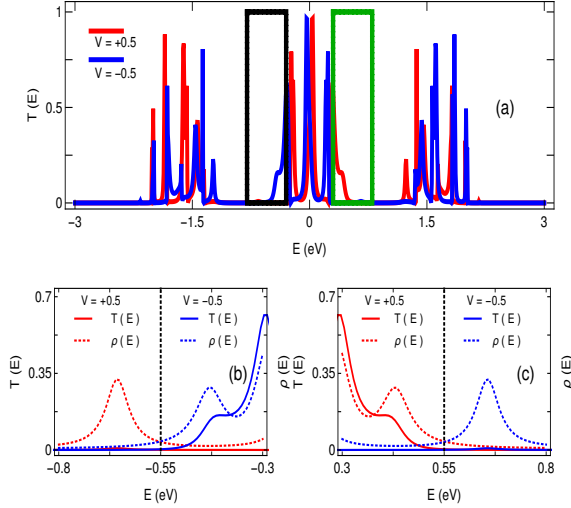


FIG. 11: (Color online). (a) Two-terminal transmission probability as a function of energy for a 15-rung ladder network under two different bias polarities considering a typical voltage strength 0.5 V. For the two selective energy zones of (a) (marked by the black and green framed regions), we re-plot the transmission function in (b) and (c) along with the ADOS for better viewing and analysis of the results. The imaginary dotted lines in these two spectra ((b) and (c)) represent the locations of equilibrium Fermi energy. The other required physical parameters for these calculations are: $t = 1$, $W_1 = 1$, $\phi_\lambda = 0$, $\tau_s = 1$, and $\tau_d = 0.6$.

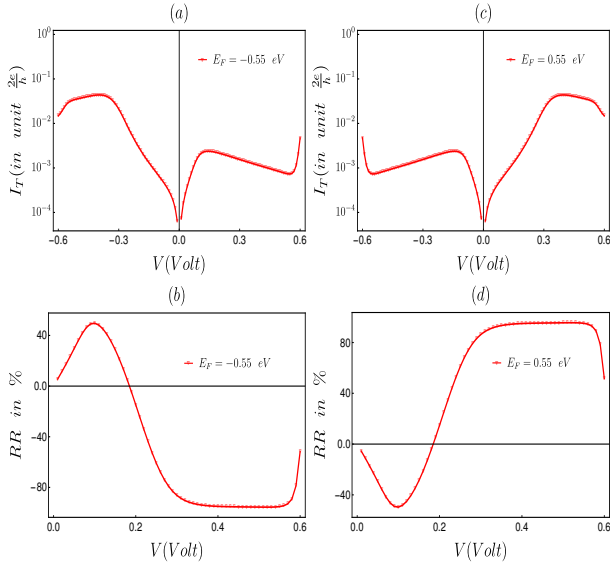


FIG. 12: (Color online). I_T - V and corresponding RR - V spectra at two different Fermi energies for the AAH ladder considering the identical physical parameters as taken in Fig. 11.

wide energy zone ($-0.8 < E < -0.3$ or $0.3 < E < 0.8$), either blue curve or the red one dominates, while the other colored curve (red or blue) almost disappears which results almost 100% rectification. As the T - E spectrum is mirror symmetric across $E = 0$, we get equal magnitude of RR , but opposite phases setting the Fermi energy

in the positive or negative side (as shown by the dotted vertical lines) across the energy band center. Comparing the transmission spectra with density of states, the WS localization can be noticed clearly.

Figure 12 shows the voltage dependence of transport current and rectification ratio for two different choices of Fermi energy ($E_F = -0.55$ eV and $E_F = 0.55$ eV). Several key features are emerged. First, the transport current is surprisingly large in one side (positive or negative) of the bias voltage, while it is almost zero in the other side of the voltage (Figs. 12(a) and (c)), and this

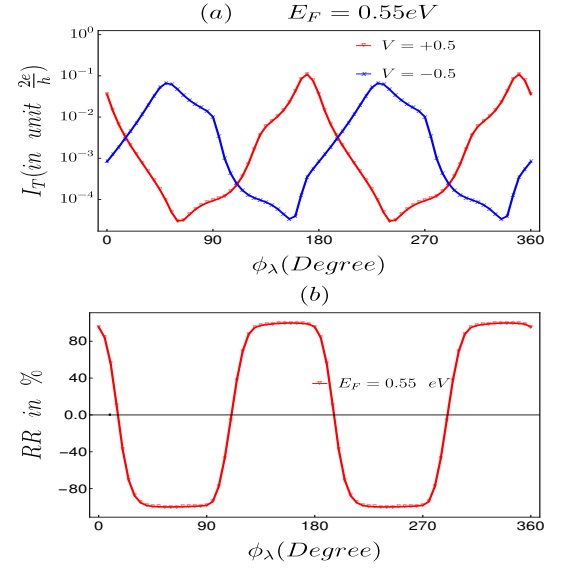


FIG. 13: (Color online). Role of AAH phase ϕ_λ on transport current and rectification ratio. In (a), transport currents are shown for two bias polarities, represented by two different colored curves, and the corresponding RR is given in (b). Here we choose $E_F = 0.55$ eV, and all the other physical parameters are kept unchanged as taken in Fig. 11.

feature persists in a reasonable voltage range (here it is $0 < V < 0.6$ V). Naturally we can expect a large rectification and it is clearly reflected from the spectra Figs. 12(b) and (d). Nearly 100% perfect rectification is obtained within the range $0.3 < V < 0.6$ V. Second, since the I_T - V spectrum is mirror symmetric across $V = 0$, a complete phase reversal takes place in the RR - V spectrum under the swapping the Fermi energy from positive zone to the negative one. Thus, a better control of rectification is expected for this AAH ladder network compared to the previous one in the main text. Third, though the current initially increases with bias voltage but it shows a decreasing nature at higher voltages (see Figs. 12(a) and (c)). Normally for the conducting junctions where bias drop takes place only at the junction points we get increasing current with voltage, as more and more contributing energy levels come within the voltage window. But for this case since the site energies are field dependent associated with the applied voltage, the site energies get modified for each bias and accordingly ADOS, and thus, transmitting peaks are shifted. As a result, the number of resonant states may decrease with increasing

voltage window which yields reducing current, exhibiting

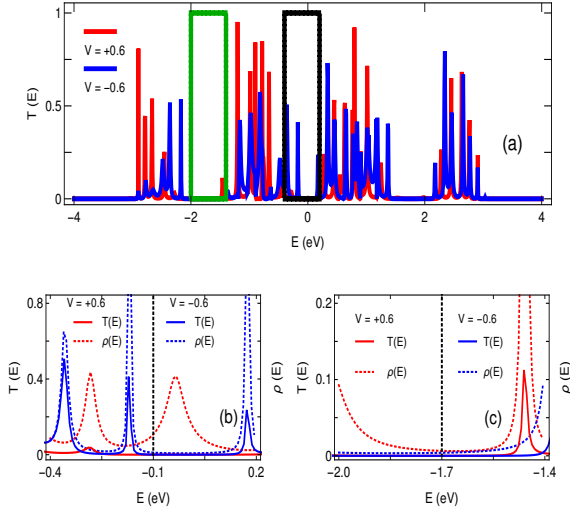


FIG. 14: (Color online). Same as Fig. 11, with $N = 21$, $W = 0.8$, $W_1 = 0.8$, $v = 1$, $t = 1$, $\phi_\lambda = \phi_\beta = 0$, $\tau_s = 1$, and $\tau_d = 0.6$. Here we fix the voltage strength at 0.6 V.

the well-known negative differential conductance (NDC) phenomenon [84].

To explore the critical role of the phase factor ϕ_λ on rectification operation for this ladder network, in Fig. 13 we present the transport currents, for two bias polarities, along with the RR as a function of ϕ_λ . Surprisingly we see that for a fixed (wide) ϕ_λ window finite current is obtained for one bias polarity, while the other becomes nearly zero, and this feature alternates with changing the phase window (see Fig. 13(a)). Due to this peculiar nature of current we get almost 100% rectification with proper phase reversal upon the variation of the AAH phase ϕ_λ . Thus, undoubtedly the AAH phase has a significant role on rectification operation.

b. AAH modulation in the onsite energy of two strands

Here, both the two strands are modulated by AAH potentials with different modulation strengths, W and W_1 , and they are expressed as: $\epsilon_{Ij}^0 = W \cos[2\pi bj + \phi_\beta]$ and $\epsilon_{IIj}^0 = W_1 \cos[2\pi bj + \phi_\beta]$. For this case we choose uniform intra-strand and inter-strand hopping integrals i.e., $t_{Ij} = t_{IIj} = t$ and $v_j = v \forall j$. In Figs. 14 - 16 we plot the transmission probabilities, dependencies of junction currents and rectification ratio with bias voltage V and phase factor ϕ_β , like the other cases. Without going into the detailed analysis of each of these spectra (Figs. 14 - 16) here we summarize the outcomes, as the essential physical mechanisms behind the rectification operations are already discussed above. It is always possible to find suitable energy window(s) where transmission function for one bias polarity significantly dominates, suppressing it in the other bias polarity (as clearly visible from the spectra Fig. 14). The complete suppression yields 100% rectification, otherwise reduced rectification ratio

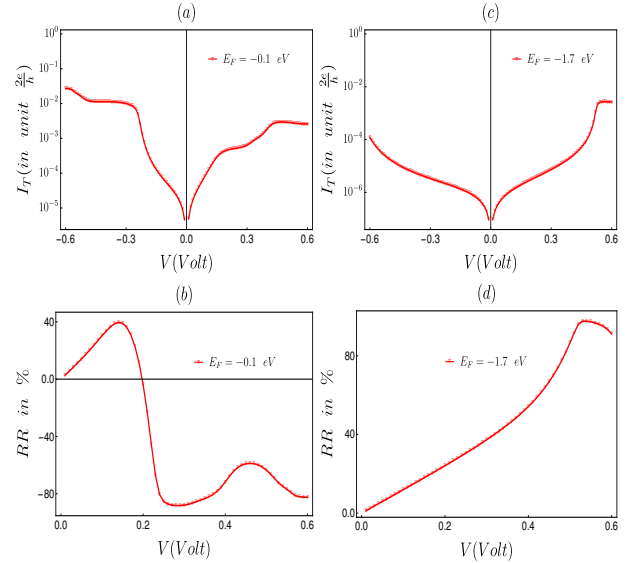


FIG. 15: (Color online). Different spectra represent the identical meanings as described in Fig. 12. The other physical parameters are same as used in Fig. 14.

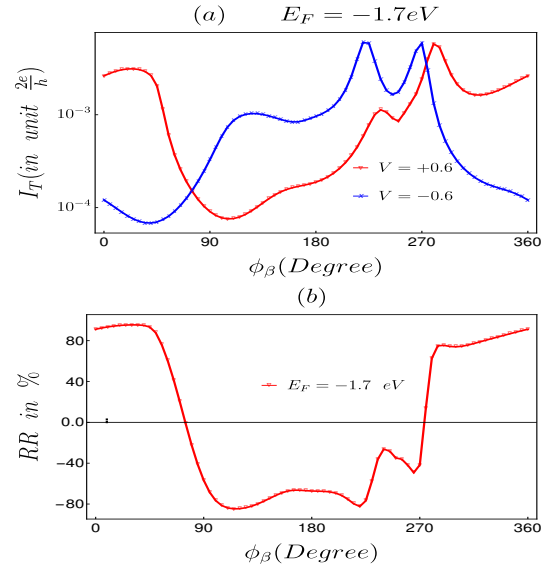


FIG. 16: (Color online). Upper and lower panels represent the similar meaning as mentioned in Fig. 6 with $E_F = -1.7$ eV and voltage strength 0.5 V. The values of the other physical parameters are same as taken in Fig. 14.

(though its large) is obtained (see Fig. 15). Two important things we need to consider for designing an efficient device those are: (i) the degree of RR and (ii) the voltage region for which the high degree of rectification persists. For this type of ladder network (case III) we can also achieve these goals. The degree of rectification can be tuned as well with the help of external phase factor ϕ_β (see Fig. 16), though in this case sequential phase reversal with almost 100% rectification in both positive and negative directions is not available like what we get in Fig. 13.

c. AAH modulation in intra strand hopping

Finally, we consider the case where the AAH modulation is introduced in the intra-strand hopping integrals, keeping uniform hopping between the two strands (viz,

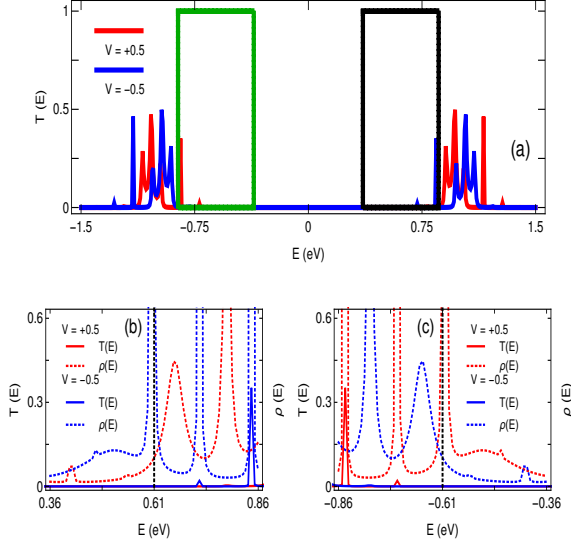


FIG. 17: (Color online). Same as Fig. 11, with $N = 15$, $\epsilon_{Ij}^0 = \epsilon_{IIj}^0 = 0$, $W = 0.4$, $W_1 = 0.4$, $v = 1$, $\phi_\lambda = \phi_\beta = 0$, $\tau_s = 1$, and $\tau_d = 0.6$.

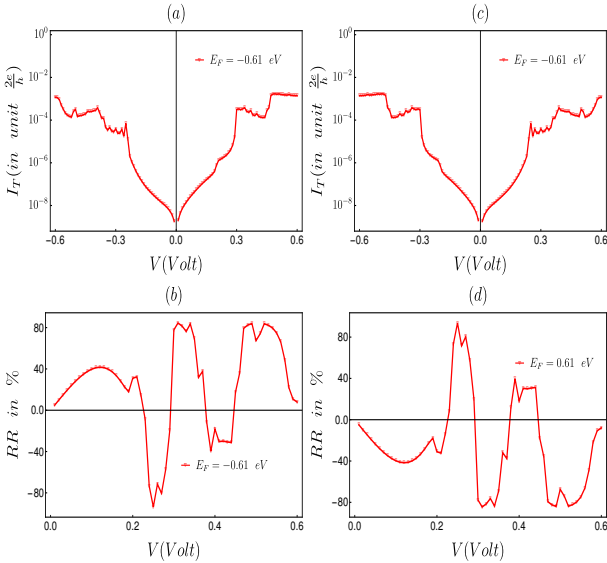


FIG. 18: (Color online). Different spectra represent the identical meanings as described in Fig. 15. The other physical parameters are same as used in Fig. 17.

$v_j = v \forall j$). Thus, for this case the intra-strand hopping integrals are described as $t_{Ij} = W \cos[2\pi bj + \phi_\lambda]$ and $t_{IIj} = W_1 \cos[2\pi bj + \phi_\lambda]$. Here, bias independent site energies are also constant and put them to zero i.e., $\epsilon_{Ij}^0 = 0$ and $\epsilon_{IIj}^0 = 0$.

Let us focus on the spectra given in Figs. 17 - 19 where the results are shown for the AAH ladder described in

this subsection. In this type of ladder, the intra-strand hopping integrals in both the upper and lower strands are modulated with AAH distributions having the strengths W and W_1 , respectively, associated with the phase factor ϕ_λ . The resonant peaks are packed together forming quasi-band like structures, and they are separated far away from each other (see Fig. 17(a)). Here also we can find some energy zones, like other cases, where one of the resonant curves associated with a particular bias polar-

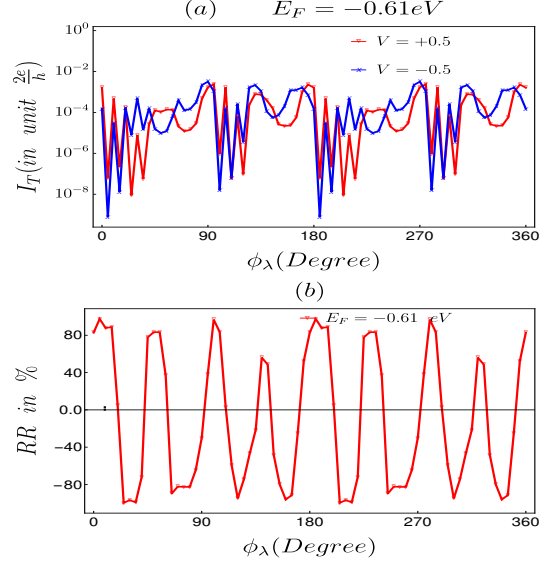


FIG. 19: (Color online). Upper and lower panels represent the similar meaning as described in Fig. 13 with $E_F = -0.61$ eV. The values of the other physical parameters are same as taken in Fig. 17.

ity dominates over the other (Figs. 17(b) and (c)), which demonstrates the possibilities of getting rectification action. For this setup the transport currents in positive and negative biases are quite low and nearly equal in the low bias region (see Figs. 18(a) and (c)) resulting smaller degree of current rectification. Whereas, reasonably large degree of rectification is achieved in the limit of higher voltage ($V > \sim 0.25$ V) associated with the I_T - V characteristics. Setting into this moderate voltage region if we tune the phase factor ϕ_λ , choosing a suitable Fermi energy, we can see that several phase windows (relatively small widths) are available where transport current for one bias polarity dominates over the other, and the dominating nature i.e., which curve dominates the other depends on the phase factor (see Fig. 19(a)). As a result of this, nice oscillating pattern is generated in RR upon the variation of ϕ_λ (Fig. 19(b)), providing high degree of rectification.

Appendix B: Combined effect of ϕ_β and ϕ_λ on rectification

The results described above in different configurations initiate the obvious curiosity that how the results of rectification depend on the two phases if we vary them to-

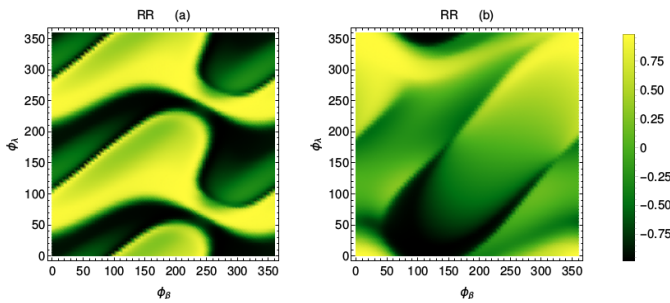


FIG. 20: (Color online). RR as functions of ϕ_λ and ϕ_β for two typical ladders. (a) $\epsilon_{Ij}^0 = W \cos[2\pi bj + \phi_\beta]$ and $\epsilon_{IIj}^0 = W_1 \cos[2\pi bj + \phi_\beta]$; $v_j = v_0 \cos[2\pi bj + \phi_\lambda]$; $t_{Ij} = t_{IIj} = t \forall j$, and (b) $\epsilon_{Ij}^0 = W \cos[2\pi bj + \phi_\beta]$ and $\epsilon_{IIj}^0 = W_1 \cos[2\pi bj + \phi_\beta]$; $t_{Ij} = t_{IIj} = t_0 \cos[2\pi bj + \phi_\lambda]$; $v_j = v \forall j$. For the calculations we choose (a) $W = W_1 = 0.5$, $v_0 = 1$, $t = 1$, $E_F = -0.7$ and (b) $W = W_1 = 0.4$, $v_0 = 1$, $t_0 = 0.4$, $E_F = 1.5$. The other parameter values are: $N = 13$ and bias voltage $V = 0.4$ V.

gether. To unravel it, in Fig. 20 we plot (density plot) the RR s for two typical AAH ladders as functions of ϕ_λ and

ϕ_β . These ladders are quite different than the previously mentioned cases, as here we consider ϕ_λ along with ϕ_β in the Hamiltonian. The two ladder systems are specified as follows: in one case (the results of which are shown in Fig. 20(a)) the upper and lower strands are subjected to AAH potentials having the strengths W and W_1 , respectively, with the phase modulation factor ϕ_β . Along with this, the AAH modulation is also introduced in the inter-strand hopping integrals with unit strength, associated with the phase factor ϕ_λ , keeping the intra-strand hopping integrals uniform. For the other ladder system (results of which are given in Fig. 20(b)), the two strands together with intra-strand hopping integrals are modulated in the AAH form, keeping the inter-strand hopping integrals as uniform. The results in both these two cases are quite interesting as we can see that for a wide range of the phase factors almost 100% rectification is available and with changing these phases the sign alteration also takes place sequentially providing the same degree of rectification.

-
- [1] A. Nitzan and M. A. Ratner, *Science* **300**, 1384 (2003).
 [2] N. J. Tao, *Nature Nanotech.* **1**, 173 (2006).
 [3] S. V. Aradhya and L. Venkataraman, *Nature Nanotech.* **8**, 399 (2013).
 [4] A. Aviram and M. A. Ratner, *Chem. Phys. Lett.* **29**, 277 (1974).
 [5] P. E. Kornilovitch, A. M. Bratkovsky, and R. S. Williams, *Phys. Rev. B* **66**, 165436 (2002).
 [6] J. Taylor, M. Brandbyge, and K. Stokbro, *Phys. Rev. Lett.* **89**, 138301 (2002).
 [7] M. Paulsson, F. Zahid, and S. Datta, *Handbook of Nanoscience, Engineering, and Technology* (2003).
 [8] R. M. Metzger, *Acc. Chem. Res.* **32**, 950 (1999).
 [9] M. Elbing, R. Ochs, M. Koentopp, M. Fischer, C. von Hanisch, F. Weigend, F. Evers, H. B. Weber, and M. Mayor, *Proc. Natl. Acad. Sci. U.S.A.* **102**, 8815 (2005).
 [10] I. Diez-Perez, J. Hihath, Y. Lee, L. Yu, L. Adamska, M. A. Kozhushner, I. I. Oleynik, and N. Tao, *Nature Chemistry* **1**, 635 (2009).
 [11] J. Hihath, C. Bruot, H. Nakamura, Y. Asai, I. Diez-Perez, Y. Lee, L. Yu, and N. Tao, *ACS Nano* **5**, 8331 (2011).
 [12] E. Lörtscher, B. Gotsmann, Y. Lee, L. Yu, C. Rettner, and H. Riel, *ACS Nano* **6**, 4931 (2012).
 [13] A. Batra, P. Darancet, Q. Chen, J. S. Meisner, J. R. Widawsky, J. B. Neaton, C. Nuckolls, and L. Venkataraman, *Nano Lett.* **13**, 6233 (2013).
 [14] T. Kim, Z. F. Liu, C. Lee, J. Neaton, and L. Venkataraman, *Proc. Natl. Acad. Sci. U. S. A.* **111**, 10928 (2014).
 [15] A. Batra, J. S. Meisner, P. Darancet, Q. Chen, C. Steigerwald, M. L. Nuckolls, and L. Venkataraman, *Faraday Discussions* **174**, 79 (2014).
 [16] B. Capozzi, J. Xia, O. Adak, E. J. Dell, Z.-F. Liu, J. C. Taylor, J. B. Neaton, L. M. Campos, and L. Venkataraman, *Nat. Nanotechnol.* **10**, 522 (2015).
 [17] A. Dhirani, P. -H. Lin, P. Guyot-Sionnest, R. W. Zehner, and L. R. Sita, *J. Chem. Phys.* **106**, 5249 (1997).
 [18] C. Zhou, M. R. Deshpande, M. A. Reed, L. Jones, and J. M. Tour, *Appl. Phys. Lett.* **71**, 611 (1997).
 [19] J. Frantti, V. Lantto, S. Nishio, and M. Kakihana, *Phys. Rev. B* **59**, 12 (1999).
 [20] G. J. Ashwell, W. D. Tyrrell, and A. J. Whittam, *J. Am. Chem. Soc.* **126**, 7102 (2004).
 [21] C. A. Nijhuis, W. F. Reus, and G. M. Whitesides, *J. Am. Chem. Soc.* **132**, 18386 (2010).
 [22] S. K. Yee *et al.*, *ACS Nano* **5**, 9256 (2011).
 [23] H. J. Yoon *et al.*, *J. Am. Chem. Soc.* **136**, 17155 (2014).
 [24] K. Wang, J. Zhou, J. M. Hamill, and B. Xu, *J. Chem. Phys.* **141**, 054712 (2014).
 [25] B. Capozzi *et al.*, *Nano Lett.* **14**, 1400 (2014).
 [26] M. L. Perrin, E. Galán, R. Eelkema, J. M. Thijssen, F. Grozema, and H. S. J. van der Zant, *Nanoscale* **8**, 8919 (2016).
 [27] X. Chen, M. Roemer, L. Yuan, W. Du, D. Thompson, E. D. Barco, and C. A. Nijhuis, *Nat. Nanotech.* **12**, 797 (2017).
 [28] J. T. Obodo, A. Murat and U. Schwingenschlögl, *Sci. Report* **7**, 7324 (2017).
 [29] M. D. Ventra and Y. V. Pershin, *Nature Nanotech.* **6**, 198 (2011).
 [30] J. C. Genereux and J. K. Barton, *Nature Chem.* **1**, 106 (2009).
 [31] G. I. Livshits *et al.*, *Nature Nanotech.* **9**, 1040 (2014).
 [32] C. Dekker and M. A. Ratner, *Phys. World* **14**, 29 (2001).
 [33] A. Guo and Q.-F. Sun, *Phys. Rev. B* **86**, 115441 (2012).
 [34] C. Guo *et al.*, *Nature Chem.* **8**, 484 (2016).
 [35] A. M. Guo, *Phys. Rev. E* **75**, 061915 (2007).
 [36] H. Lei, J. Chen, G. Nouet, S. Feng, Q. Gong, and X. Jiang, *Phys. Rev. B* **75**, 205109 (2007).
 [37] M. Saha and S. K. Maiti, *Physica E* **93**, 275 (2017).
 [38] E. Maciá, *Phys. Rev. B* **74**, 245105 (2006).
 [39] G. Cuniberti, E. Maciá, A. Rodríguez, and R. A. Römer, in *Charge Migration in DNA: Perspectives from Physics, Chemistry and Biology* edited by T. Chakraborty, Springer-Verlag, Berlin (2007).
 [40] S. Sil, S. K. Maiti, and A. Chakraborty, *Phys. Rev. Lett.* **101**, 076803 (2008).

- [41] S. Sil, S. K. Maiti, and A. Chakrabarti, *Phys. Rev. B* **78**, 113103 (2008).
- [42] E. L. Albuquerque, U. L. Fulco, V. N. Freire, E. W. S. Caetano, M. L. Lyra, and F. A. B. F. deMoura, *Phys. Rep.* **535**, 139 (2014).
- [43] L. M. Bezerril, D. A. Moreir, E. L. Albuquerque, U. L. Fulco, E. L. de Oliveira, and J. S. de Sousa, *Phys. Lett. A* **373**, 3381 (2009).
- [44] S. Maiti, S. Sil, and A. Chakrabarti, *Ann. Phys. (N. Y.)* **382**, 150 (2017).
- [45] S. Aubry and G. Andre, *Ann. Isr. Phys. Soc.* **3**, 133 (1980).
- [46] Y. E. Kraus, Y. Lahini, Z. Ringel, M. Verbin, and O. Zilberberg, *Phys. Rev. Lett.* **109**, 106402 (2012).
- [47] M. Verbin, O. Zilberberg, Y. E. Kraus, Y. Lahini, and Y. Silberberg, *Phys. Rev. Lett.* **110**, 076403 (2013).
- [48] M. Schreiber, S. S. Hodgman, P. Bordia, H. P. Lüschen, M. H. Fischer, R. Vosk, E. Altman, U. Schneider, and I. Bloch, *Science* **349**, 842 (2015).
- [49] H. P. Lüschen, S. Scherg, T. Kohlert, M. Schreiber, P. Bordia, X. Li, S. D. Sarma, and I. Bloch, *Phys. Rev. Lett.* **120**, 160404 (2018).
- [50] H. P. Lüschen, P. Bordia, S. S. Hodgman, M. Schreiber, S. Sarkar, A. J. Daley, M. H. Fischer, E. Altman, Immanuel Bloch, and U. Schneider, *Phys. Rev. X* **7**, 011034 (2017).
- [51] M. Atala, M. Aidelsburger, M. Lohse, J. T. Barreiro, B. Paredes, I. Bloch, *Nature Phys.* **10**, 588 (2014).
- [52] A. Purkayastha, S. Sanyal, A. Dhar, and M. Kulkarni, *Phys. Rev. B* **97**, 174206 (2018).
- [53] S. Ganeshan, K. San, and S. Das Sarma, *Phys. Rev. Lett.* **110**, 180403 (2013).
- [54] S. Ganeshan, J. H. Pixley, and S. Das Sarma, *Phys. Rev. Lett.* **114**, 146601 (2015).
- [55] A. Purkayastha, A. Dhar, and M. Kulkarni, *Phys. Rev. B* **96**, 180204 (2017).
- [56] Y. E. Kraus, Z. Ringel, and O. Zilberberg, *Phys. Rev. Lett.* **111**, 226401 (2013).
- [57] O. Zilberberg, S. Huang, J. Guglielmon, M. Wang, K. Chen, Y. E. Kraus, and M. C. Rechtsman, *Nature* **553**, 59 (2018).
- [58] M. Lohse, C. Schweizer, H. M. Price, O. Zilberberg, and I. Bloch, *Nature* **553**, 55 (2018).
- [59] M. Kohmoto, B. Sutherland, and C. Tang, *Phys. Rev. B* **35**, 1020 (1987).
- [60] G. J. Jin, Z. D. Wang, A. Hu, and S. S. Jiang, *Phys. Rev. B* **55**, 9302 (1997).
- [61] V. Balachandran, S. R. Clark, J. Gould, and D. Poletti, *Phys. Rev. Lett.* **123**, 020603 (2019).
- [62] D. S. Fisher and P. A. Lee, *Phys. Rev. B* **23**, 6851 (1981).
- [63] S. Datta, *Electronic Transport in Mesoscopic Systems*, Cambridge University Press, Cambridge (1997).
- [64] S. Datta, *Quantum Transport: Atom to Transistor*, Cambridge University Press, Cambridge (2005).
- [65] B. K. Nikolić and P. B. Allen, *J. Phys.: Condens. Matter* **12**, 9629 (2000).
- [66] P. Dutta, S. K. Maiti, and S. N. Karmakar, *J. Appl. Phys.* **114**, 034306 (2013).
- [67] M. Dey, S. K. Maiti, and S. N. Karmakar, *Org. Electron.* **12**, 1017 (2011).
- [68] S. K. Pati, *J. Chem. Phys.* **118**, 6529 (2003).
- [69] V. Mujica, M. Kemp, A. Roitberg, and M. Ratner, *J. Chem. Phys.* **104**, 7296 (1996).
- [70] K. Walczak, *Phys. B* **365**, 193 (2005).
- [71] A. Dey, D. S. Bhakuni, B. K. Agarwalla, and A. Sharma, arXiv:1902.00474v1.
- [72] S. Pleutin, H. Grabert, G. L. Ingold, and A. Nitzan, *J. Chem. Phys.* **118**, 3756 (2003).
- [73] S. K. Maiti and A. Nitzan, *Phys. Lett. A* **377**, 1205 (2013).
- [74] P. Dutta, S. K. Maiti, and S. N. Karmakar, *AIP Advances* **4**, 097126 (2014).
- [75] G. H. Wannier, *Phys. Rev.* **117**, 432 (1960).
- [76] J. R. Borysowicz, *Phys. Lett. A* **231**, 240 (1997).
- [77] N. Zekri, M. Schreiber, R. Ouasti, R. Bouamrane, and A. Brezini, *Z. Phys. B* **99**, 381 (1996).
- [78] I. L. Aleiner, P. W. Brouwer, and L. I. Glazman, *Phys. Rep.* **358**, 309 (2002).
- [79] C. W. J. Beenakker, *Phys. Rev. B* **44**, 1646 (1991).
- [80] M. Galperin, A. Nitzan, and M. A. Ratner, *Phys. Rev. B* **78**, 125320 (2008).
- [81] T. J. Gramila, J. P. Eisenstein, A. H. MacDonald, L. N. Pfeiffer, and K. W. West, *Phys. Rev. Lett.* **66**, 1216 (1991).
- [82] U. Sivan, P. M. Solomon, and H. Shtrikman, *Phys. Rev. Lett.* **68**, 1196 (1992).
- [83] L. Zheng and A. H. MacDonald, *Phys. Rev. B* **48**, 8203 (1993).
- [84] B. Xu and Y. Dubi, *J. Phys.: Condens. Matter* **27**, 263202 (2015).